

Steady and Unsteady Bifurcation Flows of Non-Newtonian Inelastic Fluids

H. M. Matos¹, P. J. Oliveira¹

¹Departamento de Engenharia Electromecânica, Unidade de Materiais Têxteis e Papeleiros, Universidade da Beira Interior, Rua Marques D'Ávila e Bolama, 6200-001 Covilhã, Portugal

Abstract

Steady and unsteady laminar flows in a planar 2D T-junction are studied numerically for non Newtonian inelastic fluids whose rheological characteristics are similar to those of blood. These computational fluid dynamics simulations scan variations of inertia, flow rate ratio and shear thinning, with the objective of determining the sizes of the recirculating eddies formed near the bifurcation and the resulting distribution of the shear stress fields. In hemodynamics such flow complexities are related to the genesis and development of vascular diseases, like the formation of atherosclerotic plaques and thrombi.

To represent the decay of viscosity with shear rate we apply the Carreau-Yasuda equation. In many comparisons of the present parametric study it was require that the level of inertia is approximately the same when the power law index was variable, which implies a consistent definition of the Reynolds number.

Introduction

Bifurcation flows are important in many engineering and bio-engineering applications. In engineering applications, bifurcations are commonly used in liquid distribution systems. However when the working fluid is composed by a mixture of a number of fluids and other materials like it may be found in dyeing processes in the textile industry or in the production process of paper, phase distribution in the main and the branch ducts is inevitably different, affecting the flow control and processing facilities downstream. In some situations, like in the petroleum industries, this phenomenon is advantageous and is used to accomplish the first stage of oil and gas phase separation, with attending improvement in the efficiency of the transport system [1].

Bio engineering applications are well illustrated by the hemodynamical circulatory system, in which blood flows along successive levels of arterial bifurcations producing highly complex flow patterns that promote the appearance of regions with flow separation and recirculation, which are well correlated with to the emergence and development of vascular diseases [2, 3]. Due to the highly complex flow, the endothelium wall is more easily damaged and this facilitates the macromolecules to migrate into the arterial wall, leading finally to the atherosclerotic plaque formation [4]. The interaction between blood flow and the artery wall, through the action of the fluid shear stress, is known to be extremely relevant.

Blood is a complex fluid that consists in a suspension of platelets, leucocytes and erythrocytes in plasma [5], and possesses therefore non-Newtonian properties. Blood exhibits a shear-thinning viscosity, is thixotropic and

viscoelastic [6]. Among the various non-Newtonian blood properties we concern our attention in shear thinning effects.

These computational fluid dynamics simulations scan variation of inertia, flow rate ratio and shear thinning, on steady and unsteady laminar flows in a planar 2D T-junction. Inertia effects were varied through the Reynolds number ($Re = \rho \bar{u}_t H / \eta$), from 50 to 1000. The shear-thinning viscosity follows the Carreau-Yasuda model in which the power law exponent was changed according to the intensity of viscosity variation. Finally the flow rate ratio ($\chi = Q_3 / Q_1$) varied from 0.1 to 0.9.

Numerical Simulation

Differential Equations

For the simulation of incompressible and isothermal, laminar, time-dependent flows, the equations to be solved are those expressing conservation of mass (Eq. 1) and linear momentum (Eq. 2):

$$\nabla \cdot \mathbf{u} = 0 \quad (1)$$

$$\frac{\partial \rho \mathbf{u}}{\partial t} + \nabla \cdot (\rho \mathbf{u} \mathbf{u}) = -\nabla p + \nabla \cdot \boldsymbol{\tau} \quad (2)$$

Where \mathbf{u} is the velocity, p is the pressure and ρ is the fluid density. The stress tensor in Eq. (2) is specified by a rheological constitutive model which depends on whether the fluid is Newtonian or non-Newtonian (inelastic).

For Newtonian fluids the stress tensor follows the Newton law for viscosity expressing a linear and explicit stress-strain rate relationship ($\boldsymbol{\tau} = 2\eta \mathbf{D} = \eta \dot{\boldsymbol{\gamma}}$) where \mathbf{D} is the rate-of-strain tensor, η represents the fluid viscosity and $\dot{\boldsymbol{\gamma}}$ is the shear rate tensor. For non-Newtonian inelastic fluids (Generalized Newtonian Fluids) the Carreau-Yasuda model [7] (Eq. 3) is followed to represent the viscosity variation with shear rate.

$$\eta = \eta_{\infty} + (\eta_0 - \eta_{\infty}) \left[1 + (\Lambda \dot{\gamma})^a \right]^{(n-1)/a} \quad (3)$$

In Eq. (3) η_0 and η_{∞} are the zero and infinite shear rate viscosities, Λ is a constant time and n is the power law exponent. The magnitude of these parameters is obtained from [8].

Numerical Method

We apply the finite-volume method on non-staggered meshes in which all variables are stored at the centre of cells forming the mesh [9]. The coupling between the velocity and stress fields employs the method of Oliveira et al. [10] later modified by Matos, et al. [11]. Spatial discretisation of the convective terms is accomplished with the high resolution scheme CUBISTA [12] and

temporal discretisation of the unsteady term follows the three time level scheme [13]. The pressure-correction method employed is based on the SIMPLEC algorithm.

Geometry and Computational Mesh

The simulations were carried out in a 2D T-shaped geometry (Fig. 1) having a constant cross section area with height H . The flow conditions were similar to those of Miranda et al. [6]. At the inlet a Dirichlet boundary conditions were used, by imposing a parabolic velocity profile for the steady state flows, while for transient flows the velocity profile is pulsating and generated by a sinusoidal pressure gradient:

$$-\frac{dp}{dx} = \rho K_s + \rho K_0 \cos(\omega t) \quad (6)$$

Here ρK_s is the magnitude of the steady pressure gradient and ρK_0 is the magnitude of the oscillating pressure gradient ($K_0/K_s = 2.585$). The Womersley number is $\alpha = (H(\omega/\nu)^{1/2}) = 4.864$.

At the outlets, Neumann boundary conditions were imposed. The other boundary planes are solid walls where the no slip boundary condition was imposed. The mesh is formed by 12800 control and the study of mesh refinement can be found in Matos et al. [11]. For unsteady flows the time step is 5×10^{-3} .

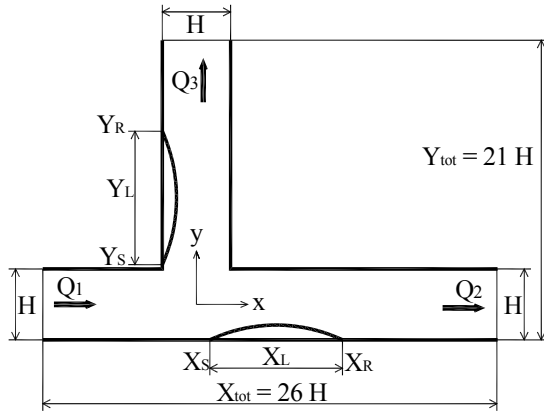


Figure 1 – Schematic representation of the simulation geometry.

Definition of effective Reynolds number

For Newtonian fluids the viscosity does not change and the Reynolds number is varied through the fluid velocity at the inlet. On the other hand for non Newtonian fluids, viscosity depends on the shear rate (Eq. 7) which affects the Reynolds number calculation and produces a hidden variation of the Reynolds number in these cases when Newtonian conditions are used.

$$Re = \frac{\rho \bar{u}_1 H}{\eta(\dot{\gamma}_1)} \text{ with } \dot{\gamma}_1 = \frac{\bar{u}_1}{H/2} \quad (7)$$

In order to maintain the effective Reynolds number constant for all cases it is necessary to adopt a modification in the calculation of Re . For this purpose in

this work we adopted an iterative procedure to determine the mean velocity that the flow must have at inlet, for an specified Reynolds number, when the corresponding viscosity of the fluid is based on the Carreau-Yasuda model, for different power law exponents, through the expression:

$$\bar{u}_1 = \frac{Re}{\rho H} \left(\eta_\infty + (\eta_0 - \eta_\infty) \left[1 + \left(\lambda 2 \bar{u}_1 / H \right)^a \right]^{\frac{n-1}{a}} \right) \quad (8)$$

During this text we adopt by default the consistent Reynolds number obtained through the iterative process defined by Eq. (8). In some results the number of Reynolds was obtained by the two methods: we refer to the “Newtonian Reynolds method” or Re_{Newt} when the Newtonian viscosity is used, and to “Modified Reynolds method” or Re_{Mod} , when the viscosity is obtained from the Carreau-Yasuda model and defined in a consistent way.

Results and Discussion

The results presented are normalised, using as length scale the channels height H , as velocity scale the average velocity of the inlet flow (\bar{u}_1), as stress scale the value of the wall shear stress at inlet under fully-developed steady flow ($\tau_{w1} = 6\eta\bar{u}_1/H$), and the ratio $2\pi/\omega$ for time scale.

In the stress scale the characteristic viscosity depends on fluid; for Newtonian and GNF fluids with the Newtonian Reynolds method, the Newtonian viscosity is used, while for GNF fluids with the Modified Reynolds method the viscosity is obtained from the Carreau-Yasuda model at $\dot{\gamma}_1 = \bar{u}_1/(0.5H)$.

The principal dependent variables in these study are the recirculation lengths of both eddies created in the main and branch arms (Fig. 1), and the shear stress fields.

Steady flow

Figures 2 and 3 show simultaneously the variation with inertia and flow rate ratio of the horizontal and vertical recirculation lengths. For the horizontal recirculation length we compare the solution obtained with the Newtonian fluid and the non Newtonian fluids (GNF) using both the “Newtonian Reynolds method” and the “Modified Reynolds method”. For the vertical recirculation length only the Modified Reynolds method is presented.

Both recirculation lengths X_L and Y_L increase monotonically with Reynolds number. The eddy in the horizontal branch increases linearly with Reynolds number for flow rate ratios lower than 0.8. The increase in the vertical eddy length is not linear for all extraction ratios due to the interaction of the main vertical recirculation with a new recirculation formed immediately downstream, in the opposite side wall of the secondary branch, which acts as to squeeze the first and delay its growth.

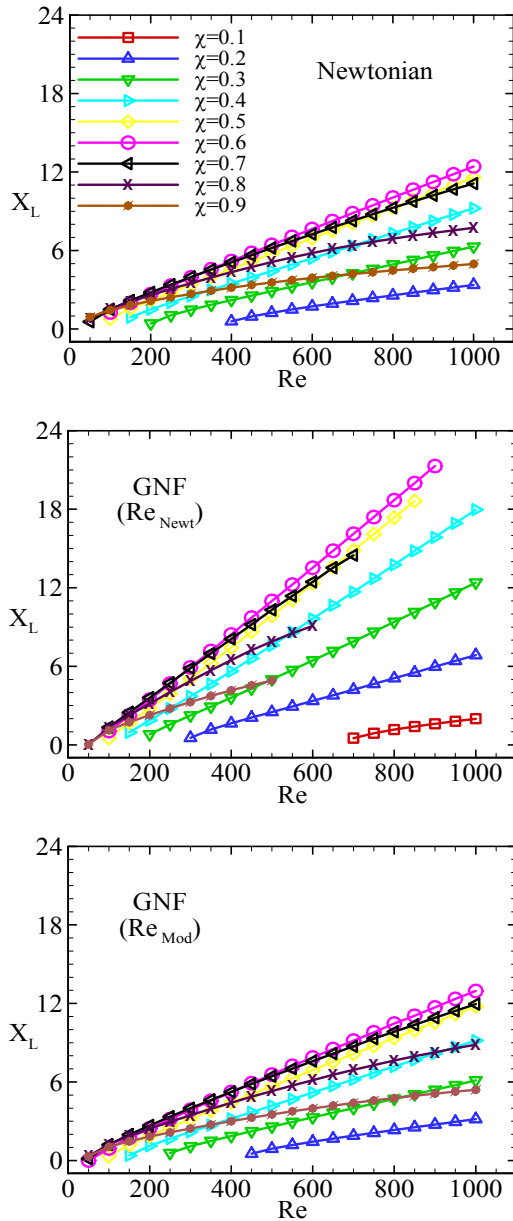


Figure 2 – Horizontal recirculation length as a function of inertia (Re) and extraction ratio (χ) for Newtonian and GNF fluids.

Figures 2 and 3 also show an increase in length with extraction ratio up to a maximum for $\chi=0.6$, while for higher values of extraction, the size of the eddies decrease.

The GNF fluids induce somewhat longer recirculation lengths for both recirculations with the Newtonian Reynolds method define Re such differences in recirculation lengths are artificially accenjuated, especially for high Reynolds numbers, when the Newtonian and non Newtonian viscosity magnitudes become very different. With the consistent definition of Reynolds number of the modified method the results for Newtonian and GNF fluids are very similar, thus demonstrating that the non-Newtonian shear thinning

effect could be accounted for by the inertial effect when the Reynolds number is obtained in a consistent way.

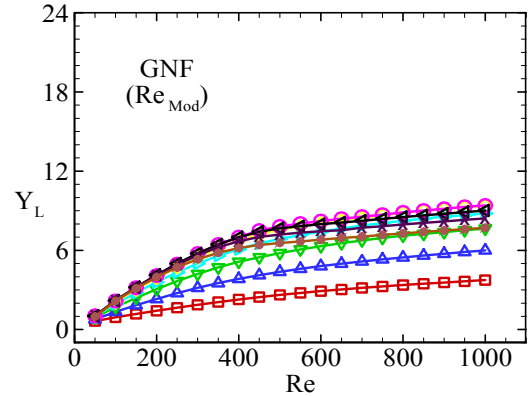


Figure 3 – Vertical recirculation length as a function of inertia (Re) and extraction ratio (χ) for the GNF (Re_{Mod}) case.

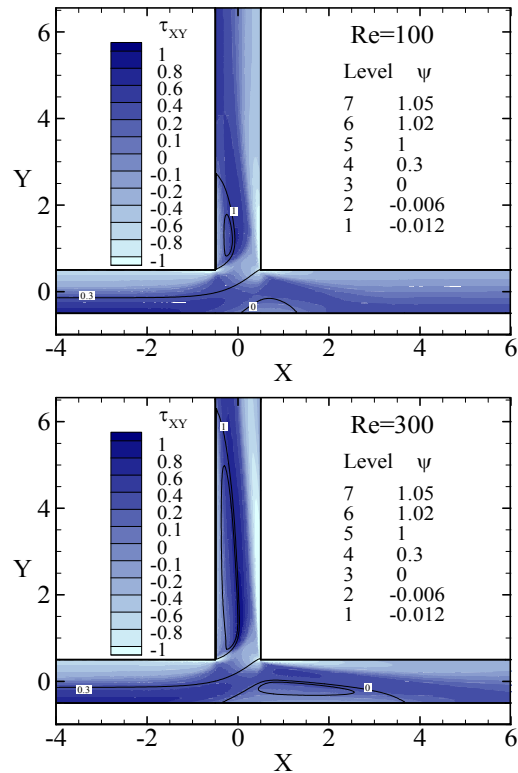


Figure 4 – Shear stress fields for increasing Reynolds numbers, at $\chi=0.7$; GNF (Re_{Mod}) case.

Figure 4 presents the evolution of shear stress with inertia for two Reynolds numbers ($Re=100$ and $Re=300$). The shear stress magnitude increases with inertia, but there always exist areas of very low shear stress close to the wall in the recirculation zones, while high stresses are generated in the recirculation boundaries, located in the main and the side branches. Such distribution induces high stress gradients and the possibility of shear stress oscillations, in space and time, which may facilitate the inflammatory process and the triggering of an atherosclerotic plaque. In general a comparison of the

stress fields between the Newtonian and the GNF fluids shows only minor differences with the Newtonian case presenting higher shear stress fields (in modulus) when compared with GNF fluids.

Figure 5 shows the evolution of the shear stress field with flow rate ratio. The flow rate ratio promotes a slight increase of maximum shear stress magnitudes (in modulus). It is noted that for low extraction ratios the higher shear stresses are registered along the main duct in the wall layer, while for high extraction ratios they are registered along the secondary branch. The maximum magnitudes occur where layers of fluid having high and low velocities come into contact, which results in increased local shearing of the flow.

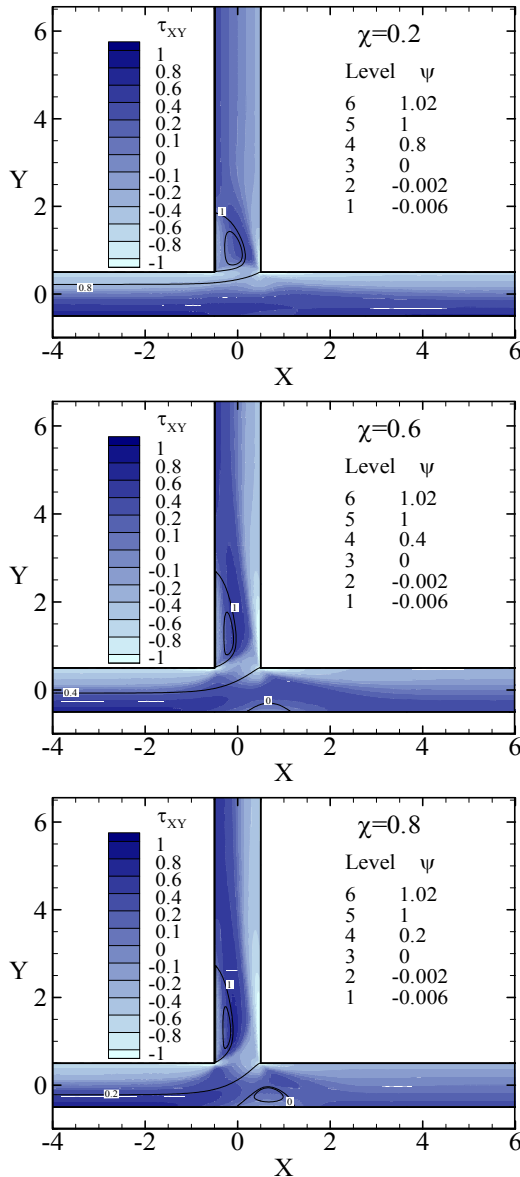


Figure 5–Shear stress fields for increasing extraction ratio, at $Re = 100$; GNF (Re_{Mod}) case.

The influence of shear thinning variation on the two eddy lengths is presented in figure 6 using the Modified

Reynolds method. When the Reynolds number is defined in a consistently way the shear thinning variation promote only slight differences, noting, however, smaller lengths for the Newtonian case ($n = 1$).

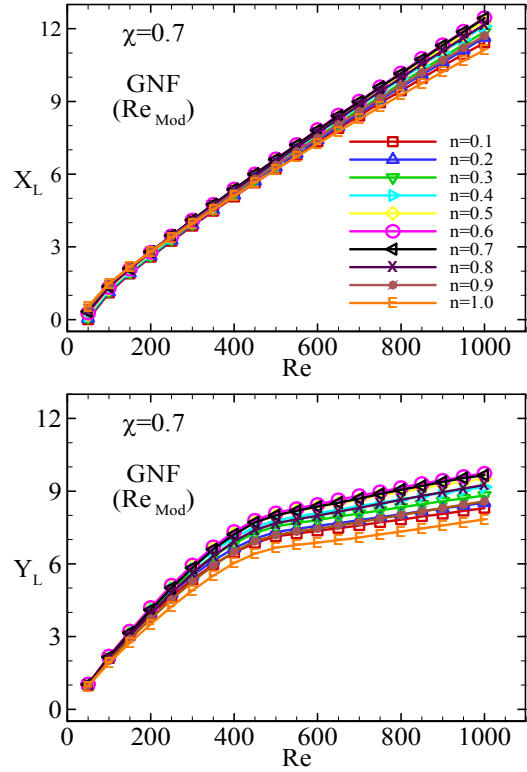


Figure 6 – Variation of X_L and Y_L with shear thinning and Re for GNF fluids with Newtonian Reynolds method and $\chi = 0.7$.

The influence of shear thinning variation does not promote the existence of large variations in the shear stress field. The shear stress variation is not monotonous, initially the increase in the power law index results in a decrease in modulus of the shear stress magnitudes to minimum values that occur for ($n \approx 0.6$). After that they increase to the maximum shear stress magnitudes that occur for the Newtonian case ($n = 1$), as shown by the maximum and minimum values registered in table 1, for different power law index.

Table 1 – Maximum and minimum shear stress for various power law indices.

Power law index	n=0.2	n=0.4	n=0.6	n=0.8	n=1
$\tau_{XY_{Max}} / \tau_{wl}$	1.22	1.15	1.11	1.18	1.35
$\tau_{XY_{Min}} / \tau_{wl}$	-7.25	-6.44	-5.76	-6.20	-8.40

Unsteady flow

All the results presented in this section were obtained at constant inertia, with $Re = 102$.

For unsteady periodic flows the recirculation lengths and shear stresses also change during the cycle. In figure 6 we

present the variation during the cycle of the separation and reattachment points of both recirculations using the GNF fluid (Re_{Mod}).

This figure shows that the horizontal recirculation is not present during the whole cycle, while the vertical recirculation is always present. However, in the latter case an abrupt reduction in length occurs after the middle of the cycle, which is associated with the breakup of the recirculation into two vortices due to the emergence of a new bubble near the wall. This phenomenon is seen by contrasting the red line (square symbols), which corresponds to the first reattachment point (unique before the division), and the purple line (circular symbols) which corresponds to the second separation point associated with a second recirculation that tends to disappear later in the cycle.

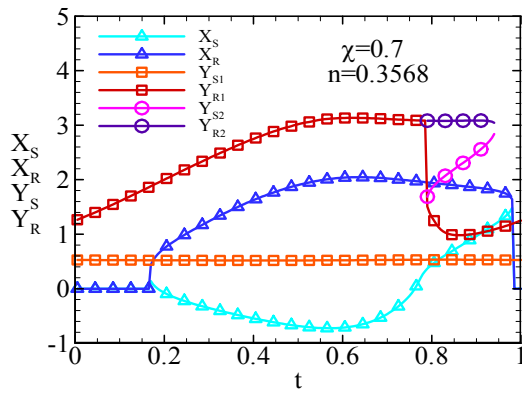


Figure 6 – Variation of the separation and reattachment points ($\chi = 0.7$; $n = 0.3568$).

The following figures show the influence of shear thinning and extraction ratio upon the recirculation lengths. Figure 7 show the influence of shear thinning variation at constant flow rate ratio ($\chi = 0.7$) and figure 8 shows the influence of flow rate ratio at constant shear thinning intensity ($n = 0.3568$).

Just as occurred in the case of steady flows (Figure 6) the increase of shear-thinning (decrease of n) does not affect significantly the results, resulting in slight increase of both X_L and Y_L recirculation lengths. For the horizontal recirculation, shear thinning also results in shorter residence times over the cycle, while the vertical recirculation tends to split earlier.

The flow rate ratio affects significantly the magnitude of the eddy lengths. The horizontal recirculation length reaches its maximum magnitude near the middle of the cycle and in this part of the cycle it presents a behaviour similar to what was registered for steady state flows. It tends to increase initially with the flow rate ratio, to a maximum that occurs at $\chi \approx 0.6$, followed by a decrease for higher flow rate ratios.

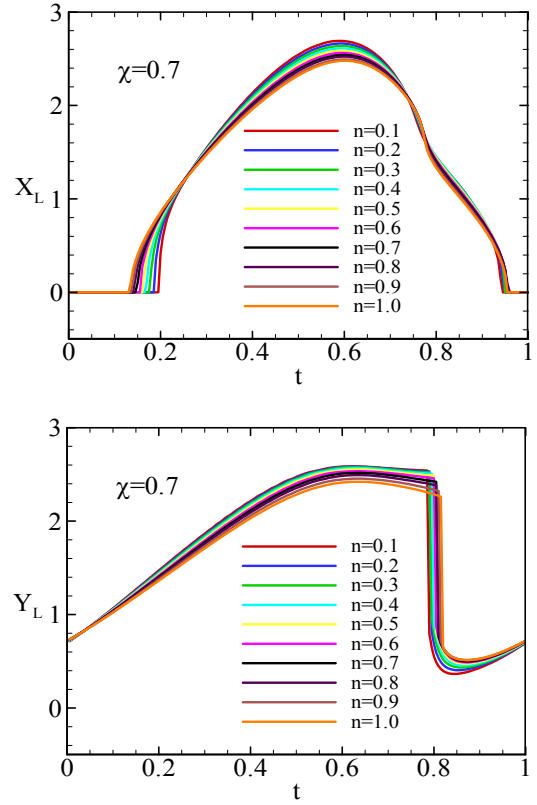


Figure 7 – Variation of recirculation lengths with n .

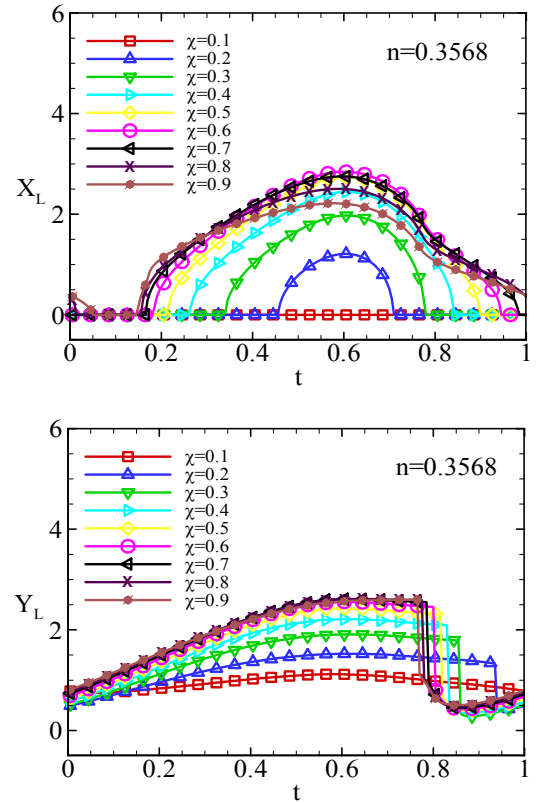


Figure 8 – Variation of recirculation lengths with extraction ratio.

For the specific shear thinning intensity here used ($n=0.3568$) there is no recirculation in the main branch for very low flow rate ratios. Increasing the flow rate ratio promotes the appearance of the horizontal recirculation, whose residence time increases monotonically with extraction ratio.

The vertical recirculation length is seen to increase with flow rate ratio, however the rate of increase is reduced as flow rate ratio increases. Furthermore the increase of flow rate ratio also tends to anticipate the division of the vertical recirculation and, for very low flow rate ratios, such division does not occur.

The variation of the shear stress field with extraction ratio presents a similar behaviour to what was observed in the case of steady flows: there is a slight increase of the maximum shear stress magnitudes (in modulus) with extraction rate. The location of the maximum shear stresses in modulus tends to occur in the branch where fluid attains larger velocities over the stagnated standing eddy.

For unsteady flows shear thinning does not promote significant variations in the shear stress fields like it was observed for steady flows. However in this case the variation is monotonous, with an increase in the shear stress field as the power law index is raised, as seen by the maximum and minimum values registered in table 2, for different power law index.

Table 2 – Maximum and minimum shear stress for various power law indices.

Power law index	n=0.2	n=0.4	n=0.6	n=0.8	n=1
$\tau_{XY_{Max}}/\tau_{w1}$	3.99	4.39	5.14	6.60	9.50
$\tau_{XY_{Min}}/\tau_{w1}$	-2.61	-2.87	-3.67	-4.12	-5.50

Conclusions

Numerical simulations were conducted for flow in a two-dimensional bifurcation with Newtonian and non-Newtonian inelastic fluids.

For non-Newtonian flows it was necessary to define the Reynolds number in a consistent way in order to maintain the same inertia as in corresponding Newtonian cases. This was done by including the shear thinning effects on the viscosity used in the Reynolds number calculation.

The comparison between Newtonian and non Newtonian fluids show that GNF fluids tend to present longer recirculation lengths in the main and the side branches and reduced shear stress field magnitudes. In steady flows the influence of shear thinning does not result in a monotonous behaviour in the recirculation lengths and shear stress fields variation, while for unsteady flows the behaviour is almost monotonous. An increase of the power law exponent results in a decrease of both recirculation lengths and an increase of the shear stress magnitudes.

Flow rate ratio, for both steady and unsteady flows, does not show a monotonous behaviour. In steady state flows,

the recirculation lengths increase with flow rate ratio up to a maximum values at $\chi=0.6$, and decrease after that. For unsteady flows this behaviour is much less pronounced and it is only registered for the horizontal recirculation in the middle of the cycle. In the case of the vertical recirculation, the maximum value is obtained for $\chi=0.7$ during part of the cycle.

For both fluids the maximum magnitudes of shear stresses present a slightly increase with flow rate ratio and the location changes with flow rate ratio variation; high shear stress magnitudes occur in the branch in the shear layer outside the recirculation eddy.

References

1. Margaris, P.D., Chem. Eng. Proc., 46(2), 150, 2007.
2. Ku, D., Annu. Rev. Fluid Mech., 29, 399, 1997.
3. Berger, S.A. and Jou, L-D., Annu. Rev. Fluid Mech., 32, 347, 2000.
4. Crowther, M.A., Hematology, (1), 436, 2005.
5. Anand, M. and Rajagopal, K. R., Int. J. Cardiovasc. Med. Sci., 4(2), 59, 2004.
6. Miranda A.I.P., Oliveira P.J. and Pinho F.T., Int. J. Numer. Meth. Fluids, 57(3), 295, 2008.
7. Carreau, P.J. Trans. Soc. Rheol., 16(1), 99, 1972.
8. Banerjee, R.K., Cho, Y.I. and Kensey, K.R., Int. J. CFD, 9(1), 23, 1997.
9. Oliveira, P.J., Ph.D. Thesis, University of London, 1992.
10. Oliveira, P.J. and Pinho, F.T., Numer. Heat Transfer B, 35(2), 295, 1999.
11. Matos, H.M.M., Alves, M.A. and Oliveira P.J., Numer. Heat Transfer B, 56(5), 351, 2009.
12. Alves, M.A., Oliveira, P.J. and Pinho, F.T., Int. J. Numer. Meth. Fluids, 41(1), 47, 2003.
13. Oliveira, P.J., J. Non-Newt. Fluid Mech., 101 (1-3), 113, 2001.

Acknowledgements

H.M. Matos wishes to acknowledge the financial support provided by FCT through the grant SFRH/BD/18062/2004.